Technical Paper

Transactions of the Society of Naval Architects of Korea
Vol. 32, No. 3, August 1995
大 韓 造 船 學 會 論 文 集
第 32 卷 第 3 號 1995年 8月

A Computational Study on Vortex Shedding around a Hydrofoil

by

Wu Joan Kim*

날개 주위의 비정상 박리 현상에 관한 연구

김 우 전*

Abstract

A numerical method was developed to solve the Navier-Stokes equations for unsteady laminar flow around a hydrofoil. The present method used the finite-difference scheme in the collocated grid system and the pressure-Poisson method was employed to obtain divergence-free velocity field each time step. The numerical method was applied at first to laminar flow around a circular cylinder to confirm capability of the code. In the next, calculations were carried out for a hydrofoil in an unbounded fluid at the Reynolds number of 10^4 in order to investigate unsteady phenomena with vortex shedding. The calculated results showed reasonable features about laminar vortex shedding around a streamlined body.

요 약

비정상 층류 유동을 위한 수치 계산법이 개발되었다. 정규 격자계와 유한 차분법이 이용되었고, 압력-Poisson 방법을 이용하여 매시간 지배 방정식을 만족하는 속도장이 구해졌다. 우선 계산 방법의 검증을 위해 원통 주위의 유동이 계산되었고, 그리고 날개 단면 주위에서 자연적으로 발생하는 비정상 박리 형상을 계산하였다. 계산 결과는 유선형 물체 주위의 층류 박리의 비정상성을 잘 보여주고 있다.

Manuscript received : March 13, 1995, Received manuscript received : June 9, 1995

* Member, Korea Research Institute of Ships & Ocean Engineering

1. Introduction

In numerical simulation or modeling of viscous incompressible flows, much effort has been directed to obtaining steady-state solutions of the unsteady Navier-Stokes equations using the so-called time-marching techniques in which time serves as an iteration parameter.

The main difficulty in calculating unsteady incompressible flows arises from the fact that the continuity equation is not a time-evolution equation, but rather a constraint that is imposed to obtain a divergence-free velocity field. Most methods for solving unsteady flow equations written in primitive variables can be classified into three groups. The first is the pressure-Poisson method, originally introduced by Harlow and Welch[1], in which a pressure equation, derived by taking the divergence of the momentum equations and requiring satisfaction of continuity equation at the new time, is solved. Recently Ohya et al.[2] used this method to calculate flow around rectangular plates. The second method is the fractional method, proposed first by Chorin[3], in which an intermediate (between the current and the new time step) velocity field is calculated from the momentum equations without a pressure gradient term, and pressure is solved to ensure that the intermediate velocity is divergence-free. This method was applied recently by Kim and Moin[4], Biringen and Danabasoglu[5], Rosenfeld et al.[6], and Hung and Moin[7]. The third method is the pseudo-time iteration (dual-time-stepping) method which was used by Soh and Goodrich[8], Rogers and Kwak[9] in conjunction with the artificial compressibility method. In this approach, iterations are performed in pseudo-time level until a divergence-free velocity field is obtained at each physical time step. Athavale[10] has recently extended the dual-time-step method to the three-dimensional unsteady flow.

In the present paper a numerical method that solves the unsteady Navier-Stokes equations using the pressure-Poisson method, based on finite-difference schemes in a collocated grid system, is presented. The time-accurate solution was sought for flow around a circular cylinder for the validation of the numerical method. Finally, the flow around a hydrofoil at the Reynolds number of 10^4 was solved to investigate naturally occurring unsteadiness with vortex shedding.

2. Numerical methods

2.1 Governing equations

In the present study only two-dimensional problems are solved, but for generality, mathematical formulation is presented in three-dimensional curvilinear coordinates using tensor notation. Consider the equations of fluid motion in Cartesian coordinates (x, y, z) for unsteady, three-dimensional turbulent flow of an incompressible fluid, where x denotes the inflow direction, y the vertical direction and origin is located at the mid-chord point of foil section. The Navier-Stokes equations, in non-dimensional form, can be written in Cartesian tensor notation as follows, where $x_i=(x, y, z)$ and $u_i=(u, v, w)$.

Continuity equation

$$\frac{\partial u_k}{\partial x_k}=o \tag{1}$$

Momentum transport equations

$$\frac{\partial u_i}{\partial t}+u_j\frac{\partial u_i}{\partial x_j}=-\frac{\partial p}{\partial x_i}+\frac{1}{Re}\nabla^2 u_i \tag{2}$$

The summation convention is used, i.e., all the terms having repeated indices such as j and k of (2) should be summed. It should be noted that, for Cartesian tensors, there is no distinction between contravariant and covariant components. The equations are non-dimensionalized by a characteristic length

L_o (chord length of a foil section (C) is chosen in the present study), a reference velocity U_o (speed of uniform incoming flow), and the density of fluid ρ. The Reynolds number is defined by $Re = U_o L_o/\nu$, where ν represents kinematic viscosity.

The grid system was generated using Knight's method[11], the details of which can be found in Kim[12]. With the body-fitted coordinate system determined, the transport equations in the physical space (x, y, z) are to be transformed into those in the computational domain (ξ, η, ζ). The governing equations in generalized coordinates are given by

Continuity equation

$$\frac{1}{J}\frac{\partial}{\partial \xi^m}(JU^m) = \frac{1}{J}\frac{\partial}{\partial \xi^m}(b_i^m u_i) = 0 \qquad (3)$$

Momentum transport equations

$$\frac{\partial u_i}{\partial t} + U^k \frac{\partial u_i}{\partial \xi^k} = -\frac{1}{J} b_i^k \frac{\partial p}{\partial \xi^k} + \frac{1}{Re}\nabla^2 u_i \qquad (4)$$

where the contravariant velocity components are defined by $U^k = \frac{1}{J} b_j^k u_j$, and the definition of geometrical coefficients can be also found in Kim[12].

2.2 Discretization

In the finite-difference schemes the derivatives with respect to spatial and temporal variables are approximated using difference forms. It is easier to represent these difference forms of the first order spatial derivative in operator notation as follows.

$$\delta_{\xi^k}^{-} = \frac{1}{6}[\ (\ )_{k-2} - 6(\ )_{k-1} + 3(\ )_k + 2(\ )_{k+1}]$$

(3rd order backward-biased)

$$\delta_{\xi^k}^{+} = \frac{1}{6}[\ -2(\ )_{k-1} - 3(\ )_k + 6(\ )_{k+1} - (\ )_{k+2}]$$

(3rd order forward-biased)

$$\delta_{\xi^k} = \frac{1}{2}[\ -(\ )_{k-1} + (\ )_{k+1}]$$

(2nd order central)

$$\delta_{\xi^k} = -(\ )_{k-\frac{1}{2}} + (\ )_{k+\frac{1}{2}}$$

(1/2-interval 2nd order central)

The convection terms are discretized using the so-called "upwind scheme" and the diffusion terms are central-differenced. The Euler-implicit method is applied for the time integration after local linearization of convection coefficients. The discretized momentum equations are

$$\frac{(u_i^{n+1} - u_i^n)}{\Delta t} + \frac{1}{2}(U^k + |\ U^k\ |)^n\ \delta_{\xi^k}^{-}(u_i^{n+1}) + \frac{1}{2}(U^k - |\ U^k\ |)^n\ \delta_{\xi^k}^{+}(u_i^{n+1}) = -\frac{1}{J} b_i^k \delta_{\xi^k}(p^{n+1}) + \frac{1}{Re}[\ g^{jj}\delta_{\xi^j}(\delta_{\xi^j}(u_i^{n+1})) + NO(u_i^n) + f^i]$$

where $NO(u_i) = g^{jk}\delta_{\xi^j}(\delta_{\xi^k}(u_i))\quad (j \neq k)$ (5)

The superscripts n, $n+1$ represents the present and the next time step, respectively. It should be noted that some of source terms are lagged.

The discretized momentum transport equations (5) were solved using a Peaceman-Rachford type ADI method until convergence for each time step. The implicit method in each direction results in the penta-diagonal matrices, for which a highly vectorized solver is available.

2.3 Velocity-pressure coupling

If the pressure is known, equation (5) can be employed to solve equations (4) for (u, v, w). However, the pressure is not known *a priori* and must be determined by requiring velocity field to satisfy the continuity equation (3). In the present study, an additional derivative of pressure is artificially added to the continuity equation to make the pressure equation solver efficient, where τ represents a pseudo-time variable for iteration process of the pressure equation and is nothing to do with the real time t. After the pressure-Poisson equation converges with pseudo-time iteration for each

physical(real) time step, the pressure field, that guarantees divergence-free velocity field in the next time step, is obtained, i.e.,

$$\frac{1}{\beta}\frac{\partial p}{\partial \tau}+\frac{1}{J}\frac{\partial}{\partial \xi^k}(b_i^k u_i) = 0 \qquad (6)$$

where β means an artificial speed of pressure wave propagation. The value of β is dependent upon flow characteristics and the numerical method and commonly taken between 0.001 and 1000. In the present calculation 1.0 was chosen after several trial-and-errors.

Once velocity components are obtained from the momentum equations, the pressure field in the next time step is obtained to project the velocity field into divergence-free one in the next time step, i.e.,

$$u_i^{n+1}=\hat{u}_i^n-\frac{\Delta t}{J}b_i^j\frac{\partial p^{n+1}}{\partial \xi^j} \qquad (7)$$

where $\hat{u}_i^n=u_i^n-\Delta t\left[U^j\frac{\partial u_i}{\partial \xi^j}-\frac{1}{Re}\nabla^2 u_i\right]^n$

Substitution of equation (7) into (6) gives

$$\frac{1}{\beta}\frac{(p^{m+1}-p^m)}{\Delta \tau}-\frac{1}{J}\frac{\partial}{\partial \xi^k}\left[\left(J\Delta t g^{kj}\frac{\partial p^{m+1}}{\partial \xi^j}\right]\right.$$

$$=-\frac{1}{J}\frac{\partial}{\partial \xi^k}\{b_i^k\hat{u}_i^n\} \qquad (8)$$

where m represents a pseudo-time or iteration time step introduced only for convenience. The pseudo-time increment $\Delta\tau$ in pressure equation (8) should be considered as an iteration variable which acts like a relaxation parameter to control the speed of change of pressure field along with β. After converging with respect to m-iteration, p^{m+1} becomes p^{n+1}. It should be mentioned again that m-th pseudo-time step is nothing to do with n-th real time step and serves only as an internal iteration loop for the given n-th real time level. Using an operator form,

$$\frac{1}{\beta}\frac{(p^{m+1}-p^m)}{\Delta \tau}+\frac{1}{J}\delta_{\xi^k}\{b_i^k\hat{u}_i^n\}$$

$$-\frac{1}{J}\delta_{\xi^k}\{J\Delta t g^{kj}\delta_{\xi^j}(p^{m+1})\}=0$$

However, the above equation has two consecutive 2nd order central differences of one-interval form appearing in the last term. This arrangement decouples pressure variables at adjacent grid locations, which results the well-known "checker-board" problem (oscillatory pressure field). The staggered grid system having four different locations for variables has been employed to avoid such a problem. However, the staggered grid system is complicated to code and is not very appropriate for the vectorization, or multi-grid acceleration since all the geometric coefficients should be stored for four different locations, otherwise calculated each time step or interpolated from adjacent values. Thus, the collocated (non-staggered or regular) grid system in which all four variables are defined at the same location is employed in the present numerical method. In the collocated grid system an extra care should be taken to avoid oscillatory pressure field.

In the present study, the fourth order artificial dissipation is added in the way of Sotiropoulos et al.[13], i.e., the spatial derivative of the pressure equation (8) is approximated using the combination of 1/2-interval and one-interval formulation as follows.

$$\frac{\partial}{\partial \xi^k}\left(J\Delta t g^{jk}\frac{\partial p^{m+1}}{\partial \xi^j}\right)$$

$$\cong(1-\varepsilon)\,Lp^{m+1}+\varepsilon\tilde{L}p^{m+1}+Np^{m+1}$$

where

$$\begin{cases} L=\delta_{\xi^k}(J\Delta t g^{kk}\delta_{\xi^k}), \quad \tilde{L}=\tilde{\delta}_{\xi^k}(J\Delta t g^{kk}\tilde{\delta}_{\xi^k}) \\ N=\delta_{\xi^k}(J\Delta t g^{jk}\delta_{\xi^j}) \quad (k\neq j) \end{cases}$$

and ε is a dissipation parameter. The dissipation is not added for $\varepsilon=0$, resulting in a one-interval formulation with an oscillatory pressure field and $\varepsilon=1$ results in a 1/2-interval formulation with the artificial dissipation of $\frac{1}{4}(J\Delta t g^{kk})\frac{\partial^4 p}{(\partial \xi^k)^4}$ approximately,

see Sotiropoulus et al.[13] for details. Thus, the resulting pressure equation is written by

$$\frac{1}{\beta}\frac{(p^{m+1}-p^m)}{\Delta\tau}-\frac{1}{J}[\ (1-\varepsilon)Lp^{m+1}$$

$$+\varepsilon\hat{L}p^{m+1}+Np^{m+1}]\ =-\frac{1}{J}\delta_{\xi^k}(b_i^k\hat{u}_i^n) \qquad (9)$$

For convenience, the delta form of the above equation is used with the definition of

$$\Delta p^{m+1}\ =\ p^{m+1}-p^m$$

Equation (9) becomes

$$\frac{1}{\beta\Delta\tau}\Delta p^{m+1}-\frac{1}{J}[\ (1-\varepsilon)\ L\Delta p^{m+1}+\varepsilon\hat{L}\Delta p^{m+1}$$

$$+N\Delta p^{m+1}]\ =-\frac{1}{J}\delta_{\xi^k}(b_i^k\hat{u}_i^n)$$

$$+\frac{1}{J}[\ (1-\varepsilon)\ Lp^m+\varepsilon\hat{L}p^m+Np^m] \qquad (10)$$

To keep tri-diagonal characteristics, put $\varepsilon=1$ only on the left-hand-side (LHS) of the equation (10) and $N(\Delta p^{m+1})$ is ignored. This approximation does not affect the converged solution since $\Delta p^{m+1}=0$ after converging for the n-th real time step. Thus (10) becomes

$$\frac{J}{\beta}\frac{\Delta p^{m+1}}{\Delta\tau}-\hat{L}(\Delta p^{m+1})\ =RHS \qquad (11)$$

$$=-\delta_{\xi^k}(b_i^k\hat{u}_i^n)+[\ (1-\varepsilon)\ Lp^m+\varepsilon\hat{L}p^m+Np^m]$$

The approximate-factorizing is applied to the left-hand-side(LHS) of (11).

$$\left\{1-\frac{\beta}{J}\Delta\tau[\ \delta_\xi(J\Delta tg^{11}\delta_\xi)]\ \right\}$$

$$\left\{1-\frac{\beta}{J}\Delta\tau[\ \delta_\eta(J\Delta tg^{22}\delta_\eta)]\ \right\} \qquad (12)$$

$$\left\{1-\frac{\beta}{J}\Delta\tau[\ \delta_\zeta(J\Delta tg^{33}\delta_\zeta)]\ \right\}(\Delta p^{m+1})=\frac{\beta}{J}\Delta\tau RHS$$

Thus, tri-diagonal matrices were solved three times in each direction to get Δp^{m+1}. After converging ($\Delta p^{m+1}=0$), $p^{n+1}=p^{m+1}$ provides the pressure field which guarantees the divergence-free velocity field at the (n+1)-th time step.

2.4 Boundary conditions

With the fully-elliptic momentum transport equations, it is necessary to specify boundary conditions on all boundaries. In the present study C-type grid topologies were chosen, thus, boundaries of the physical domain consist of an outer boundary, a body boundary, an exit and a branch cut in wake. Along the branch cut four grid points (two points from each side) were overlapped to ensure the continuous change of flow variables across the branch cut. No slip condition is applied to the foil surface since the unsteadiness naturally occurring from the body at rest is of concern in the present study. Uniform flow was specified for the outer boundary and the downstream velocities are extrapolated.

3. Results and discussion

The numerical methods described in the previous section were applied to simulate vortex shedding near a circular cylinder of the Reynolds number of 200, which is commonly considered as a test case for naturally occurring unsteadiness, to validate the numerical method. In the next, flow around a NACA0012 section of the Reynolds number 10^4 was simulated since some steady calculations appeared in the literature, although there was found some experimental evidence of vortex shedding. In the sequel, computed results are shown and discussed with an emphasis of vortex shedding.

3.1 Flow near a circular cylinder

The periodic vortex shedding behind a bluff body exposed to a uniform flow has been frequently used to test the time accuracy of numerical codes. For example, prediction of the Strouhal number of vortex shedding behind a circular cylinder was attempted by Leconite and Piquet[14], Rosenfeld et al.[15], and Rogers and Kwak[9], As a test of the present numerical method, the flow around a circular cylinder at Re=200 was considered. This

calculation started from the initial Blasius solution distributed along the cylindrical surface. No artificial triggering mechanism other than truncation error was applied. The grid was generated from the solutions of Poisson equations. A C-type grid system with 149 points in ξ-direction and 45 points in η -direction was employed, the partial view of which is shown in figure 1.

Time increment used for the present calculation was 0.025 and time history of lift and drag coefficients are shown in figure 2. It should be mentioned that time accuracy was not sought for the first 3000 iteration to reduce CPU time.

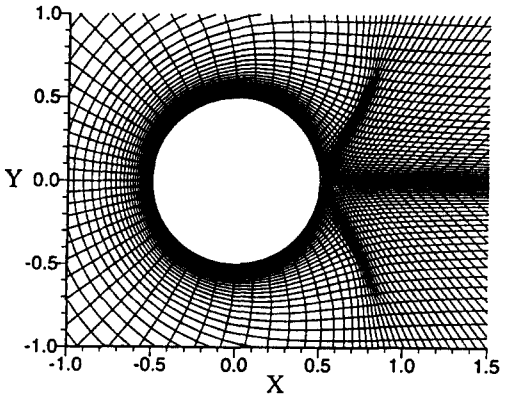

Fig.1 A partial view of grids generated for a circular cylinder

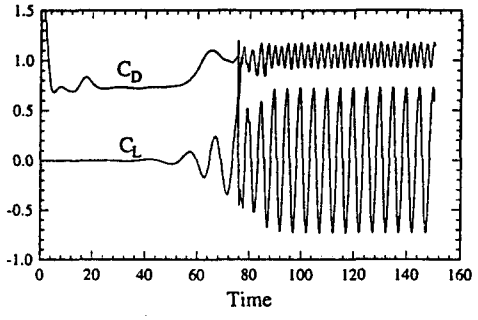

Fig.2 Time history of lift and drag coefficients of a circular cylinder at Re=200

Periodicity of the lift and drag coefficients implies the time accuracy of the present method. Lift coefficients had the period of 5, implying the Strouhal number of 0.2, while drag coefficients had the period of 2.5. Strouhal number and lift and drag coefficients are compared with experiment and other calculations in table 1. Lift coefficients and Strouhal number agreed with experiments and other calculation, although fluctuating components of the drag coefficient was overpredicted.

Table 1 Lift and drag coefficients for circular cylinder at Re=200

	C_D	C_L	St
Wille[16] (exp)	1.3		
Kovasznay[17](exp)			0.19
Roshko[8] (exp)			0.19
Lecointe&Piquet[14]	1.58±0.0035	±0.50	0.194
Rosenfeld et al.[15]	1.40±0.04	±0.70	0.201
Rogers&Kwak[9]	1.23±0.05	±0.65	0.185
The present method	1.05±0.12	±0.73	0.20

Flow patterns at the time of maximum and minimum lift are shown in figure 3 and 4. Time symmetry is observed between two figures, implying the capability of the present numerical method for unsteady flow. Streamwise velocity contours are showing a big separated region of flow reversal as denoted to by dashed lines in the figures and the trail of wake moves up and down. It is also seen that vertical velocity components have a series of sign change in wake, implying vortex shedding. Streamlines drawn from flow vectors clearly show vortex shedding behind a circular cylinder. It should be noted that flow pattern at the time of maximum lift has profiles symmetric to that of minimum lift with respect to x-axis.

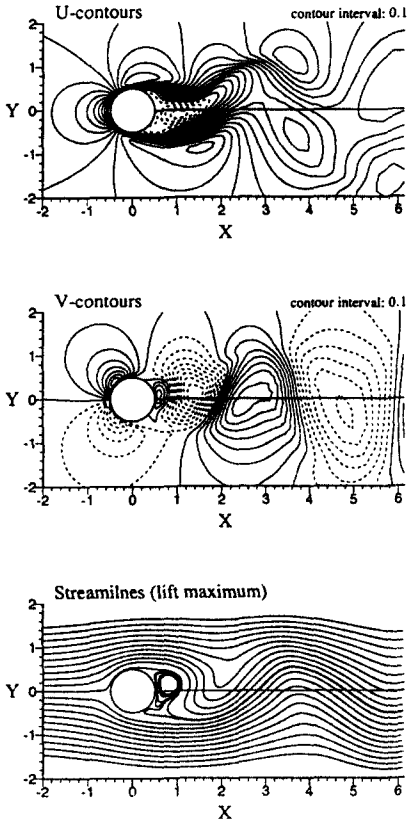

Fig. 3 Flow patterns around a circular cylinder at the time of maximum lift

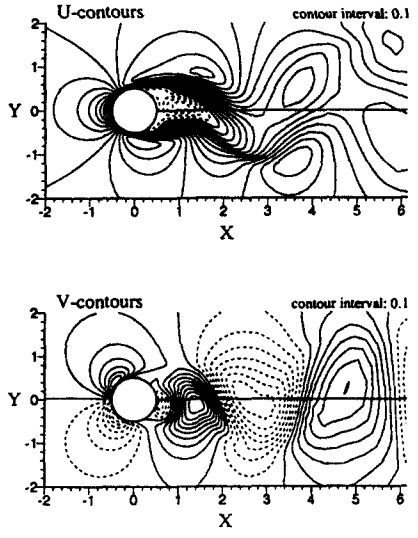

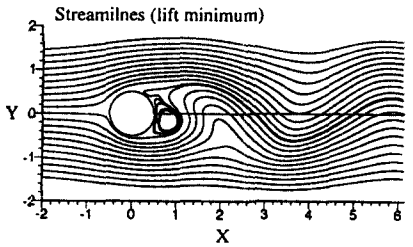

Fig. 4 Flow patterns around a circular cylinder at the time of minimum lift

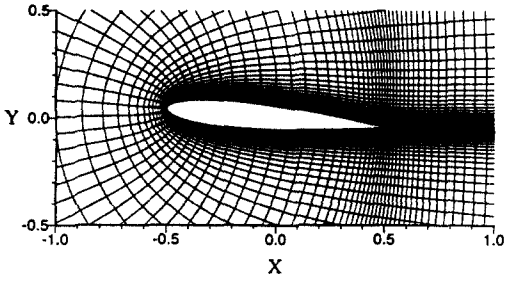

Fig. 5 A partial view of grids generated for a NACA0012 section (α=5°)

3.3 Flow around a hydrofoil

A NACA0012 section of Reynolds number 10^4 was taken as a test case in several previous studies, for example, see Obashi and Chen[19], Kim and Van[20], Lee et al.[21], and Van et al.[22]. However, most of them did not pay much attention to unsteadiness of the flow including vortex shedding. It is experimentally proven that a series of vortices are shedded behind a streamlined body as well as a bluff body for low Reynolds number. Ikehata and Suzuki[23] presented photographs showing vortex shedding phenomena around a NACA0012 and 0015 section of Reynolds number 7000 or 14000. In the present study the numerical simulation of naturally unsteady flow with vortex shedding around a NACA0012 section was carried out at the Reynolds number of 10^4.

Three angles of attack of 0° , 5° , and 10° were selected for the calculation. Figure 5 shows a partial view of grid system used for the case of $\alpha=5°$. The calculation was

carried out with 149X45 grids covering the computational domain of -5<X<7 and -5<Y<5. The lift and drag coefficients were plotted against time for the three angles of attack in figure 6.

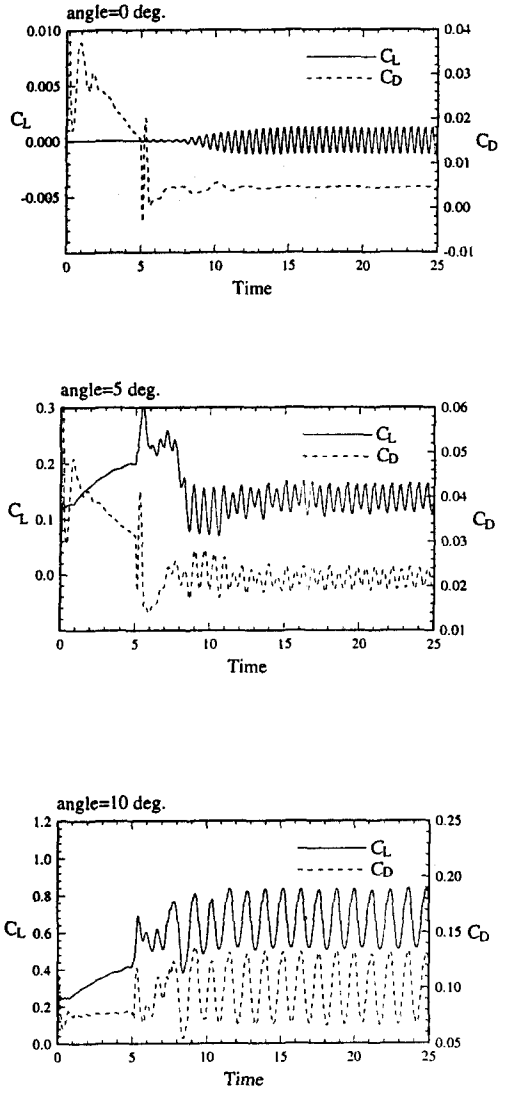

Fig. 6 Time history of lift and drag coefficients of a hydrofoil at $Re=10^4$

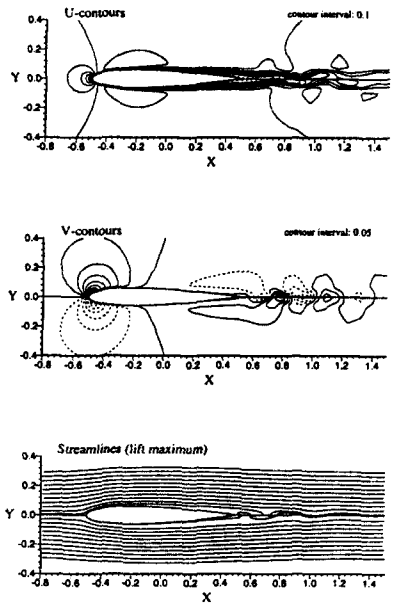

Fig. 7 Flow patterns around a hydrofoil at the time of maximum lift ($\alpha=0^\circ$)

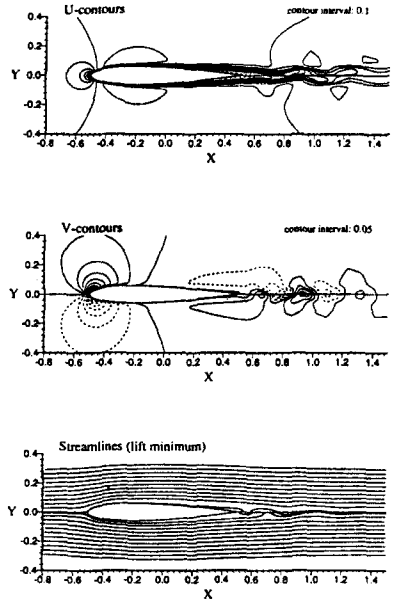

Fig. 8 Flow patterns around a hydrofoil at the time of minimum lift ($\alpha=0^\circ$)

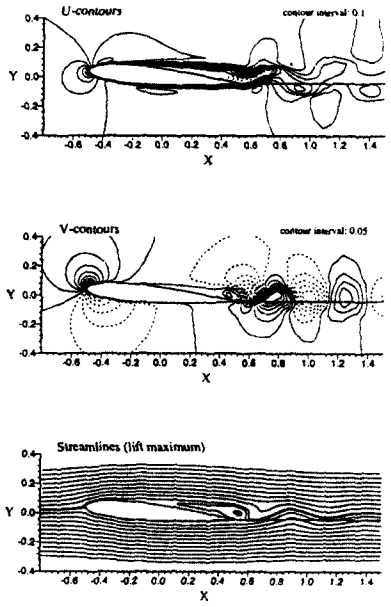

Fig. 9 Flow patterns around a hydrofoil at the time of maximum lift (α=5°)

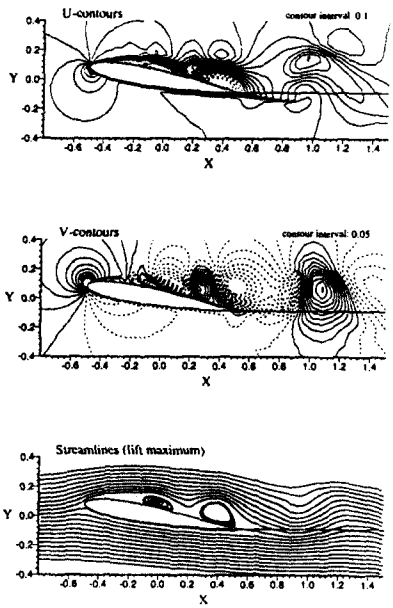

Fig. 11 Flow patterns around a hydrofoil at the time of maximum lift (α=10°)

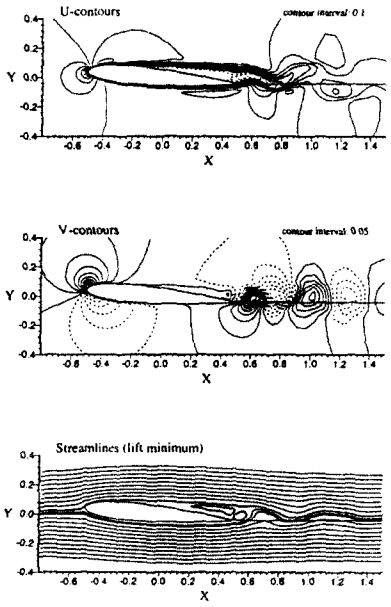

Fig. 10 Flow patterns around a hydrofoil at the time of minimum lift (α=5°)

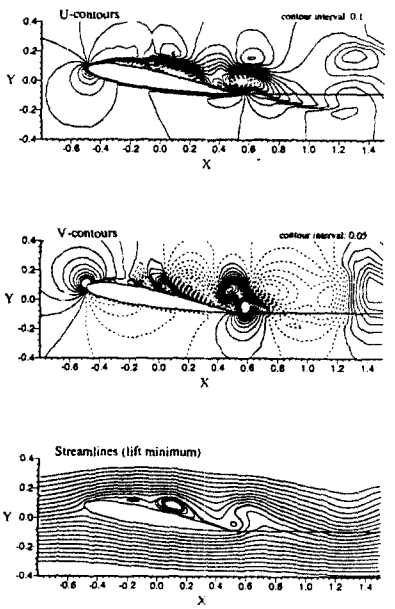

Fig. 12 Flow patterns around a hydrofoil at the time of maximum lift (α=10°)

Calculated Strouhal numbers are 2.13, 1.72, and 0.83 for 0° , 5° , and 10° , respectively. Initially Blasius solution was given and time-accurate solution was sought at each time step with the time increment of 0.01. Unsteadiness appeared at non-dimensional time of 5.0 and periodicity was observed after 15. It should be mentioned that no artificial triggering was applied other than truncation error. Flow patterns at the time of maximum and minimum lift are shown in figure 7 and 8 for $\alpha=0°$. It is clearly seen that vortices were shedded even for zero angle of attack, as noted by Ikehata and Suzuki[23]. Time symmetry of the flow was well simulated, showing the capability of the present method. Figure 9 and 10 has the flow patterns of $\alpha=5°$. The region of flow reversal is smaller at the time of maximum lift than at the time of minimum lift. It should be noted that four grid points were overlapped along the branch cut of C-type grid system in wake to ensure transfer of flow information across the branch cut. In case of $\alpha=10°$, flow pattern becomes more complicated and has stronger vortex formation, as shown in figure 11 and 12. As noted by Van et al.[22], several vortices were formulated along the suction side of foil. It is interesting that vertical velocity has strong upward components at the time of minimum lift, while it has small downward components at the time of maximum lift.

4. Concluding remarks

A numerical method for the solution of unsteady two-dimensional Navier-Stokes equations was developed. The collocated (non-staggered) grid system was employed along with the finite-difference (the 3rd order upwind-biased scheme) discretization. The time-accuracy of the solution was ensured using the pressure-Poisson method. At first, flow around a circular cylinder was solved for Re=200 to validate the present numerical method. Calculated results agreed reasonably with the experiment and other calculations. In the next, the vortex shedding around a NACA0012 section at $Re=10^4$ was simulated. It is clearly shown that flow unsteadiness can happen naturally for the laminar flow not only around a bluff body but also near a streamlined body and the present numerical method is very useful to simulate such flows.

Acknowledgement

This paper is based on the results from a Elementary Research Program (ED5540) supported by the Ministry of Science and Technology.

References

[1] Harlow, F.H., Welch, J.E., "Numerical Calculation of Time-Dependent Viscous Incompressible Flow with Free Surface," Journal of Computational Physics, Vol. 8, pp. 2182-2189, 1965

[2] Ohya, Y, Nakamura, Y., Ozono, S., Tsuruta, H., Nakamura, R., "A Numerical study of Vortex Shedding from Flat Plates with Square Leading and Trailing Edges," Journal of Fluid mechanics, Vol. 236, pp. 445-460, 1992

[3] Chorin, A.J., "Numerical Solution of the Navier-Stokes Equations," Math. Comp., Vol. 22, pp. 745-762, 1968

[4] Kim, J., Moin, P., "Application of a Fractional Step Method to Incompressible Navier- Stokes Equations," Journal of Computational Physics, Vol. 59, pp. 308-323, 1985

[5] Biringen, S., Danabasoglu, G., "Oscillatory Flow with Heat Transfer in a Square Cavity," Physics of Fluids A, Vol. 1, pp. 1796-1812, 1989

[6] Rosenfeld, M., Kwak, D., Vinokur, M., "A Fractional Step Method for the Unsteady

for the Unsteady and Incompressible Navier- Stokes Equations in generalized Coordinate Systems," Journal of Computational Physics, Vol. 94, pp. 102-137, 1991

[7] Hung, L., Moin, P., "An Improvement of Fractional Step Methods for the Incompressible Navier-Stokes Equations," Journal of Computational Physics, Vol. 92, pp. 369-379, 1991

[8] So, W.Y., Goodrich, J.W., "Unsteady Solution of Incompressible Navier-Stokes Equations," Journal of Computational Physics, Vol. 79, pp. 113-134, 1988

[9] Rogers, S., Kwak, D., "An Upwind Differencing Scheme for the Time-Accurate Incompressible Navier-Stokes Equations," AIAA-Paper 88-2583, 1988

[10] Athavale, M.M., A Numerical Scheme for Time-Accurate Solutions of Incompressible Flow Equations, Ph.D. Thesis, Penn. State Univ., College Park, 1990

[11] Visbal, M., Knight, D., "Generation of Orthogonal and Nearly Orthogonal Coordinates with Grid Control near Boundaries," AIAA Journal, Vol. 20, No. 3, 1982

[12] Kim, W.J., An Experimental and Computation Study on the Pressure Distribution around a Hydrofoil Moving under the Free Surface, Report UCE554-1845D, KRISO, 1994

[13] Sotiropoulos, F., Kim, W.J., Patel V.C. , "A Computational Comparison of Two Incompressible Navier-Stokes Solvers in Three-Dimensional Laminar Flows," Computers and Fluids, Vol. 23, No. 4, pp.627-646, 1994

[14] Lecointe, Y., Piquet, J.. "On the Use of Several Compact Methods for the Study of Unsteady Incompressible Viscous Flow around a circular cylinder," Computers and Fluids, Vol. 12, pp. 255-280, 1984

[15] Rosenfeld, M., Kwak, D., Vinokur, M., "A Solution Method for the Unsteady and Incompressible Navier-Stokes Equations in generalized Coordinate Systems," AIAA-Paper 88-0718, 1988

[16] Wille, R., "Karman Vortex Streets," Adv. Appl. Mech., Vol. 6, pp. 273, 1960

[17] Kovasznay, L.S.G., "Hot-wire Investigation for the Wake behind Cylinders at Low Reynolds Numbers," Proc. Roy. Soc. A, Vol. 198, pp. 174-190, 1949

[18] Roshko, A., On the Development of Turbulent Wakes from Vortex Streets, NACA Report 1191, 1954

[19] Obashi, K.M., Chen, C.J., Prediction of Laminar and Turbulent Flow past a Single and Twin Hydrofoils, IIHR Report No. 317, Univ. of Iowa, 1987

[20] Kim, H,T., Van, S.H., "Computation of Viscous Flow around a Two-Dimensional Foil Section," Proceedings of SNAK spring meeting, 1993

[21] Lee, H.J., Kim, H,T., Van, S.H., "Numerical Calculation of Viscous Flow around a Two-Dimensional Foil Section," Proceedings of SNAK spring meeting, 1994

[22] Van, S.H., Kim, H,T., Lee, H.J., "Numerical Computation of Viscous Flow past a Two-Dimensional Hydrofoil," Proceedings of the International Conference on Hydrodynamics, Wuxi, China, 1994

[23] Ikehata, M., Suzuki, K., "Topics of Flow Visualization in CWC of YNU," Proceeding of Korea-Japan Joint Workshop on CWC, 1994